Electronic Supplementary Material (ESI) for Journal of Materials Chemistry A.
This journal is © The Royal Society of Chemistry 2023

# Supporting information

## Monodispersed PtCo alloy nanoparticles with a modulated d-band center exhibiting highly efficient hydrogen evolution

Chengcheng Yan [a], Wei An [a], Tongjun Shen [a], Ling Ma [a], Mengyang Zhang [a], Fuming Gao[a], Tuo Yang [a], Chunxia Wang [a, *], Guoyong Huang [a, *], Shengming Xu [b]

[a] State Key Laboratory of Heavy Oil Processing, College of New Energy and Materials, China University of Petroleum (Beijing), Beijing 102249, China.

[b] Beijing Key Lab of Fine Ceramics, Institute of Nuclear and New Energy Technology, Tsinghua University, Beijing, 100084, China.

E-mail: cxwang@iccas.ac.cn; huanggy@cup.edu.cn.

## 1. Experimental materials and methods

Materials: Analytical grade cobalt nitrate hexahydrate ($Co(NO_3)_2 \cdot 6H_2O$), zinc nitrate hexahydrate ($Zn(NO_3)_2 \cdot 6H_2O$), ascorbic acid, methanol, ethanol, 2-methylimidazole and chloroplatinic acid ($H_2PtCl_6 \cdot 6H_2O$)was obtained from Aladdin Reagents Ltd. The commercial Pt/C (20%) catalyst was purchased from Tanaka, Japan. Nafion was acquired from Sigma-Aldrich. All of the chemicals used in this experiment were analytical grade and used without further purification.

Preparation of ZIF67@ZIF8, and ZIF8: The synthesis of ZIF67@ZIF8 was realized according to the previous reported method with minor modification. Typically, 2-methylimidazole (9.852 g, 120 mmol) dissolved in a mixed solution was added to 100 mL a mixed solution of methanol and 100 mL ethanol containing $Co(NO_3)_2 \cdot 6H_2O$ (1.455 g, 5.00 mmol) and $Zn(NO_3)_2 \cdot 6H_2O$ (7.437 g, 25.00 mmol) under stirring for 15 s. The mixture was kept at room temperature for 20 h. The precipitate was collected by centrifugation, washed, and dried under vacuum at 60 $^oC$ overnight. ZIF8 were synthesized by a similar procedure by substituting $Co(NO_3)_2$-$6H_2O$ with $Zn(NO_3)_2$-$6H_2O$ was replaced with for ZIF8.

Preparation of Co-NC and NC: The precursors of ZIF67@ZIF8, and ZIF8 were heated at 900 °C with a heating rate of 5 °C $min^{-1}$ for 2 h under Ar atmosphere and naturally cooled to room temperature to obtain Co-NC and NC.

Preparation of PtCo-NC and Pt-NC: 50 mg of Co-NC were ultrasonically dispersed in 35 mL of deionized water, then 440 μL of aqueous chloroplatinic acid solution (60 mg $mL^{-1}$) was added, followed by addition of 1.2 mL of aqueous ascorbic

acid solution (0.1 M) and kept for 4 h at 65 °C. Then, the products were c centrifugated, washed, and freeze-dried at 60 °C under vacuum to yield PtCo- NC. Similarly, Pt-NC was synthesized according to the same method by using NC as the raw materials.

## 2. Structural and surface characterization

X-ray diffraction (XRD) measurements were performance on a DX-2700BH X-ray diffractometer using Cu Kα radiation. The morphology and structure of the electrocatalyst were characterized using a HITACHI SU 8010 scanning electron microscopy (SEM) and a FEI Tecnai G2 F20 transmission electron microscopy (TEM). The samples were dispersed in ethanol and sonicated for 30 min and the suspension were casted onto TEM grids for TEM measurement. X-ray photoelectron spectroscopy (XPS) measurements were performed by using a K-ALPHA with Al Kα radiation. All the XPS spectra were calibrated by shifting the detected C 1s peak to 284.4 eV.

## 3. Electrochemical measurements

5 mg of the electrocatalyst and 20 μL Nafion solution (5 wt%) were dispersed in 500 μL isopropanol and 500 μL water for sonication to form a slurry. Then, 5 μL of the slurry was loaded onto the surface of a glassy carbon electrode (GCE, 3 mm in diameter), and the GCE was dried at room temperature. The electrochemical HER measurements were performed by a conventional three-electrode system on a CHI 760E electrochemical workstation (Chenhua Co., Ltd., Shanghai, China), using catalyst-covered glassy carbon (GC) electrode as the working electrode, Ag/AgCl (3 M KCl) as the reference electrode and graphite rod as the counter electrode, respectively. The electrocatalytic activity of the electrocatalyst towards HER was examined by obtaining

polarization curves using linear sweep voltammetry (LSV) at room temperature in 1 M KOH and 0.5 M $H_2SO_4$ solution at a scan rate of 5 mV $s^{-1}$. All the electrochemical data are presented without iR compensation. All the potentials reported in our work are estimated based on the following equation, which is relative to those of the reversible hydrogen electrode (RHE). $E_{RHE}=E_{Ag/AgCl}+0.059\ pH + 0.197$.

## 4. Density functional theory calculation

By employing the Vienna Ab-initio Simulation Package (VASP), free energies were computed through density functional theory (DFT). The generalized gradient approximation of Perdew, Burke and Ernzerhof (PBE) was selected for exchange-correlation potential. The kinetic energy cut-off was set at 500 eV, the total energies were converged to $1 \times 10^{-5}$ eV, the convergence criterion for the residual forces on the atoms was set to 0.05 eV Å-1 during the relaxation. A $5 \times 5 \times 1$ k-mesh was employed for the Brillouin zone integrations. All calculations were performed on a slab model with $2 \times 2$ surface cell containing five (111) atomic layers and a vacuum layer of 20 Å thickness to avoid artificial interaction between periodic images. The top layers were allowed to relax, while the bottom three layers were fixed. Hydrogen adsorption energies were calculated relative to $H_2$ (g) as

$$\Delta E = E(\text{slab} + H) - E(\text{slab}) - \frac{1}{2}E(H_2) \quad (1)$$

The associated hydrogen free energy is

$$\Delta G = \Delta E + \Delta ZPE - T\Delta S \quad (2)$$

$\Delta ZPE$ being the difference in zero-point energy and $\Delta S$ the difference in entropy between the adsorbed state and gas phase.

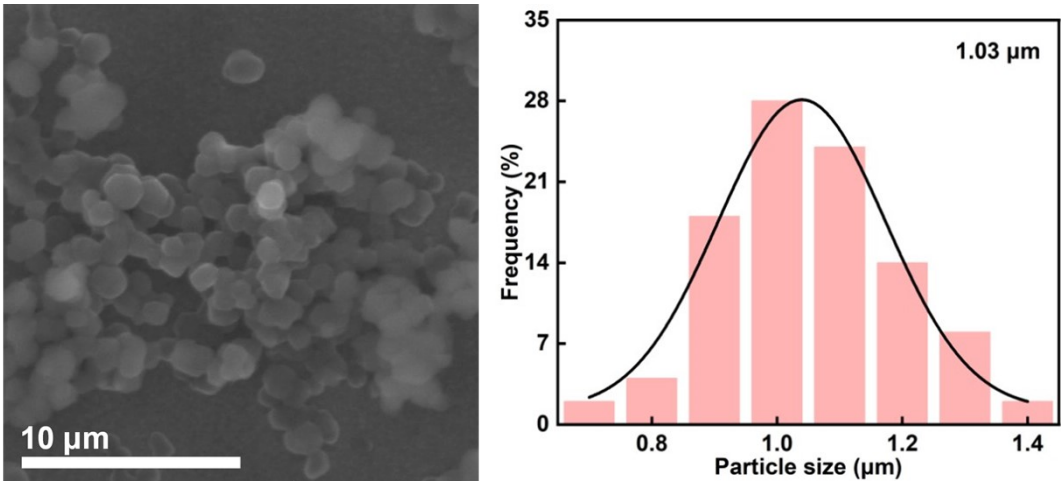


Figure S1. SEM images of ZIF67@ZIF8 and size distributions

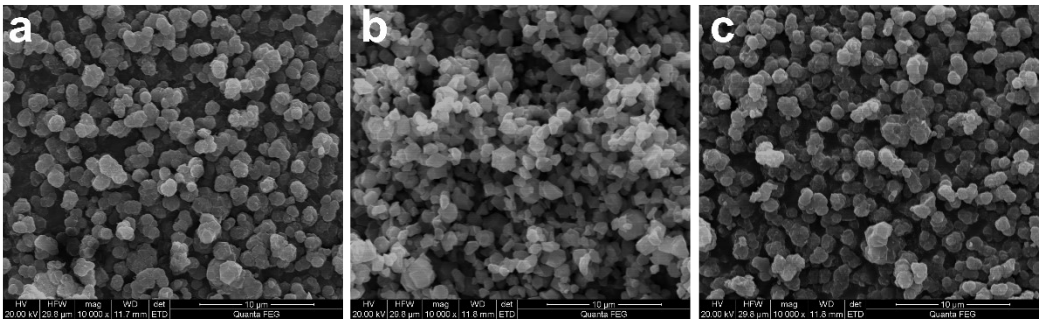


Figure S2. SEM images of Co-NC (a), Pt-NC (b) and PtCo-NC (c).

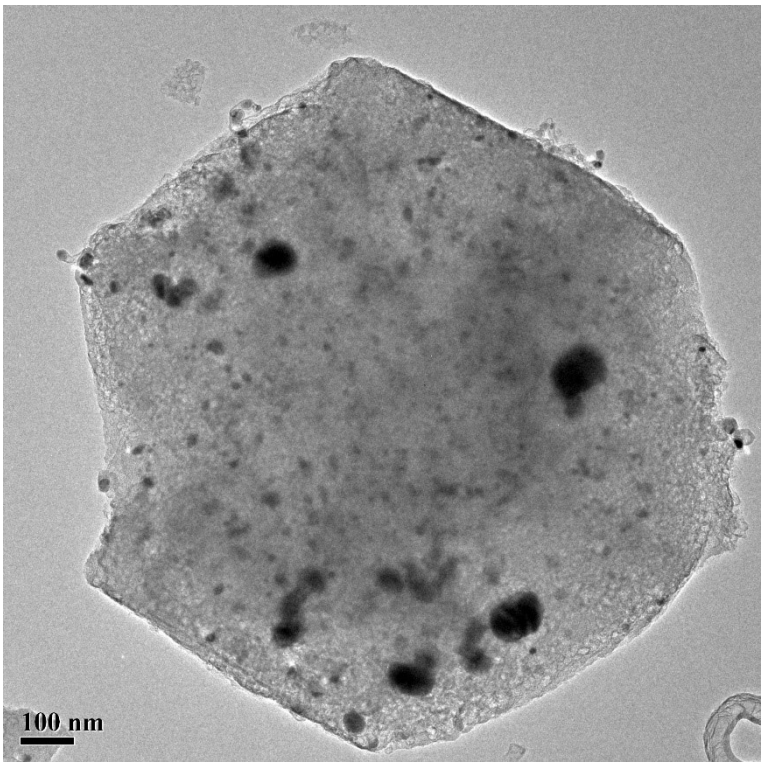


Figure S3. TEM image of Co-NC

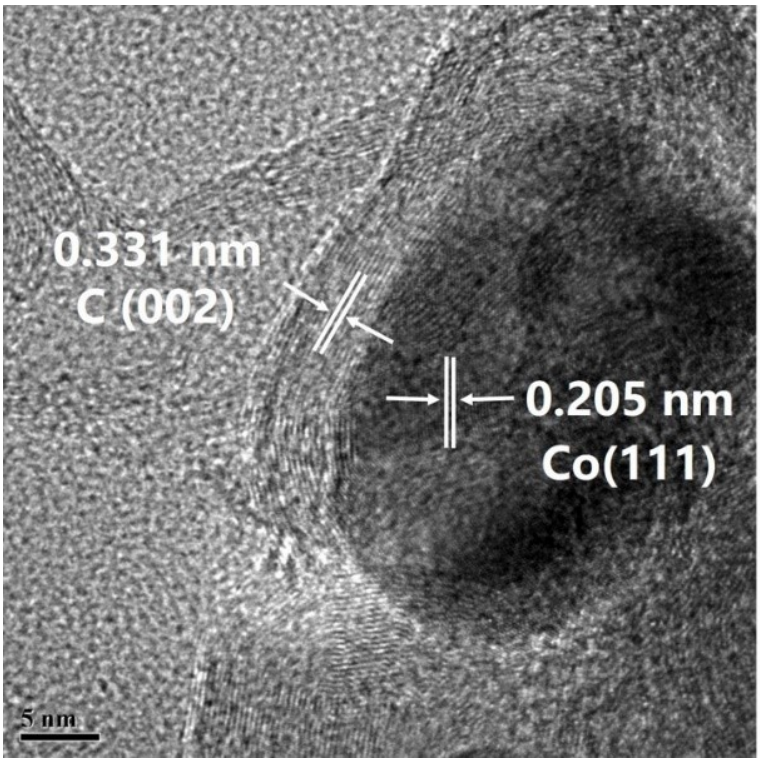


Figure S4. Magnifying HRTEM image of Co-NC

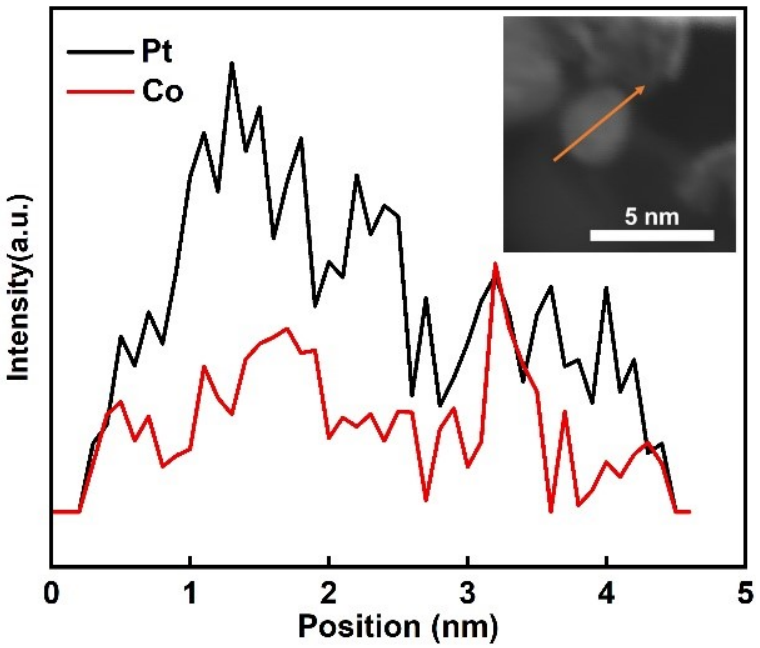


Figure S5. EDX line-scan analysis result for the selected PtCo-NC in the direction of the orange arrow

Table S1. The atomic percentage of PtCo-NC determined by EDX elemental mapping

| Element | Atomic number | Mass [%] | Normalized mass[%] | Atomic [%] | Abs. error [%](1 sigma) | Rel. error [%](1 sigma) |
|---|---|---|---|---|---|---|
| Carbon | 6 | 93.85 | 93.85 | 98.78 | 2.95 | 3.14 |
| Nitrogen | 7 | 0.81 | 0.81 | 0.73 | 0.05 | 6.61 |
| Cobalt | 27 | 0.57 | 0.57 | 0.12 | 0.08 | 8.11 |
| Zinc | 30 | 0.00 | 0.00 | 0.00 | 0.00 | 0.00 |
| Platinum | 78 | 4.36 | 4.36 | 0.37 | 0.55 | 12.58 |
| | Total: | 100.00 | 100.00 | 100.00 | | |

Table S2. The content of Pt, Co, and Zn in the PtCo-NC electrocatalysts determined by ICP-OES

| Samples | Pt(wt%) | Co(wt%) | Zn(wt%) |
|---|---|---|---|
| PtCo-NC | 16.21 | 1.63 | - |

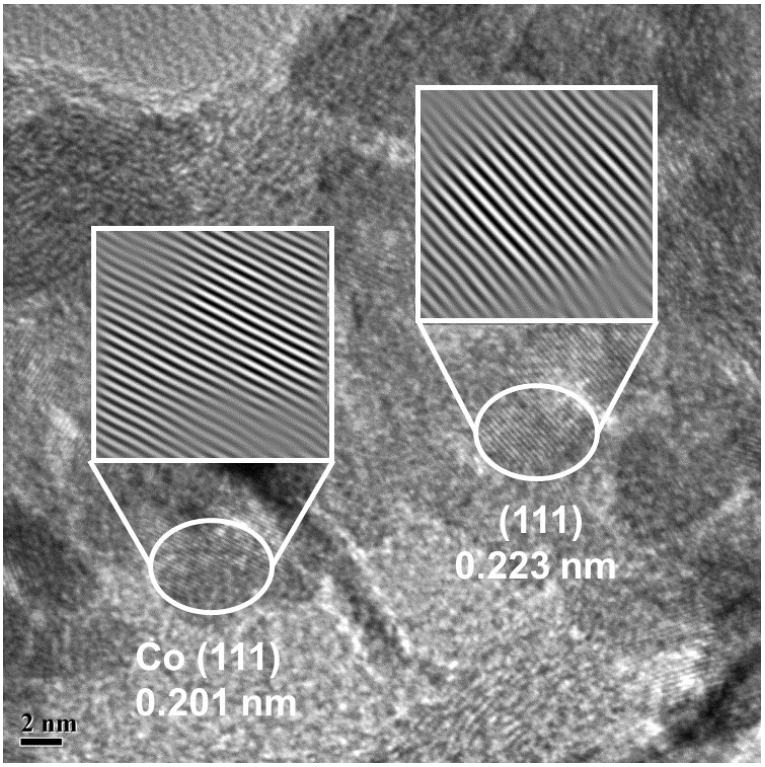


Figure S6. Magnifying HRTEM image of PtCo-NC

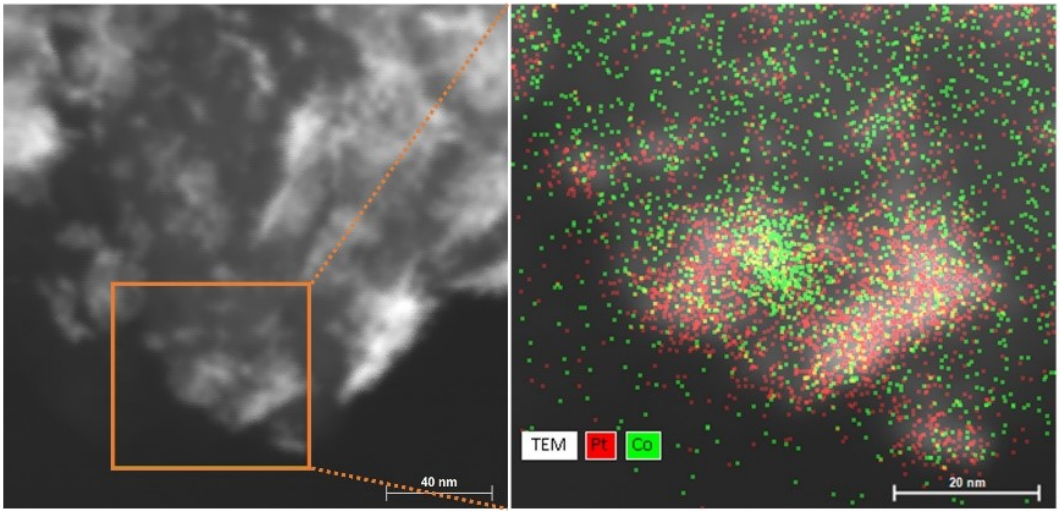


Figure S7. EDX element mapping of PtCo-NC

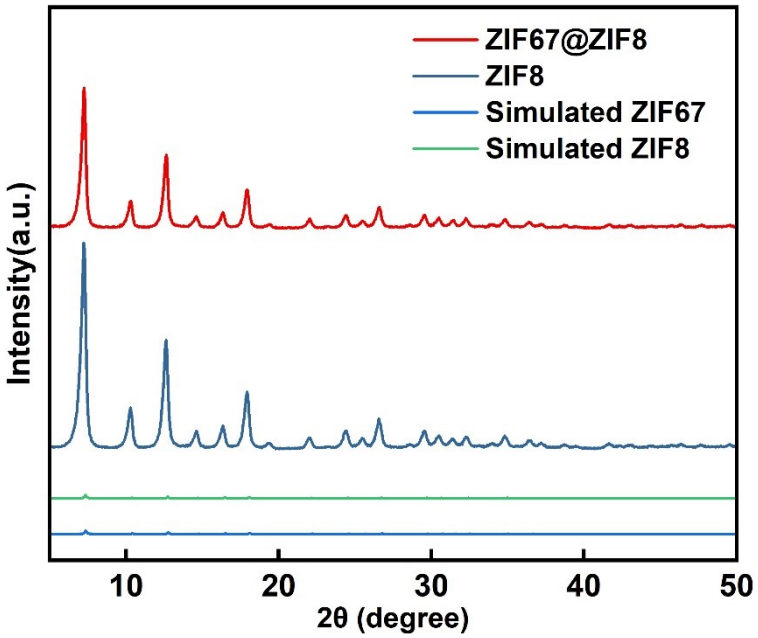


Figure S8. X-ray diffraction patterns of ZIF67@ZIF8 and ZIF8

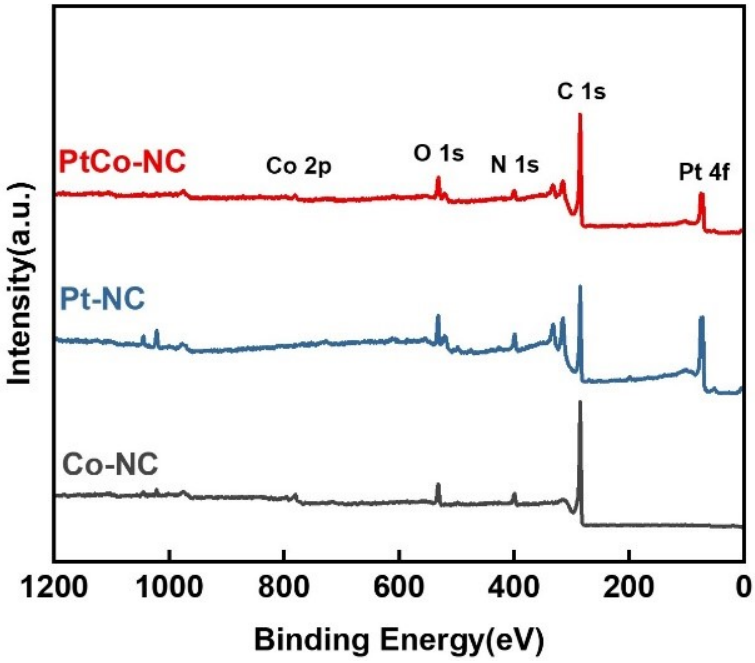


Figure S9. XPS survey of PtCo-NC, Pt-NC and Co-NC

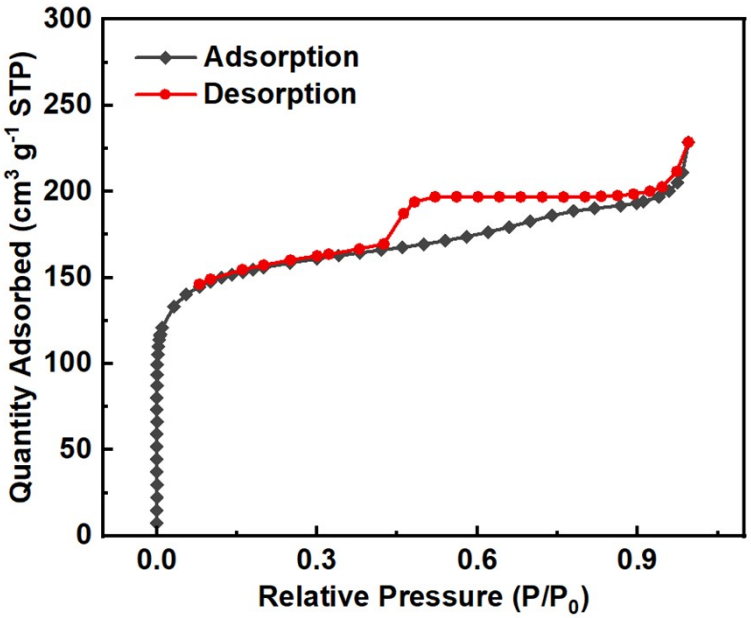


Figure S10. $N_2$ adsorption–desorption isotherms of PtCo-NC

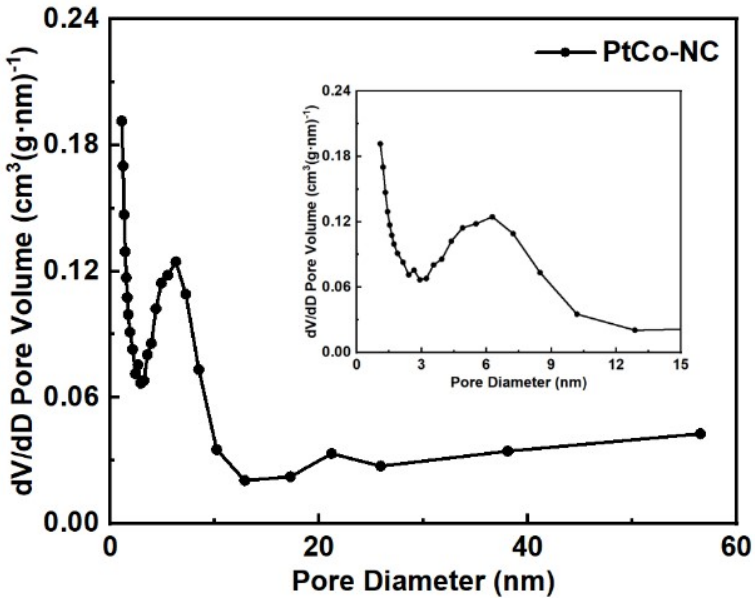


Figure S11. Pore size distributions of PtCo-NC

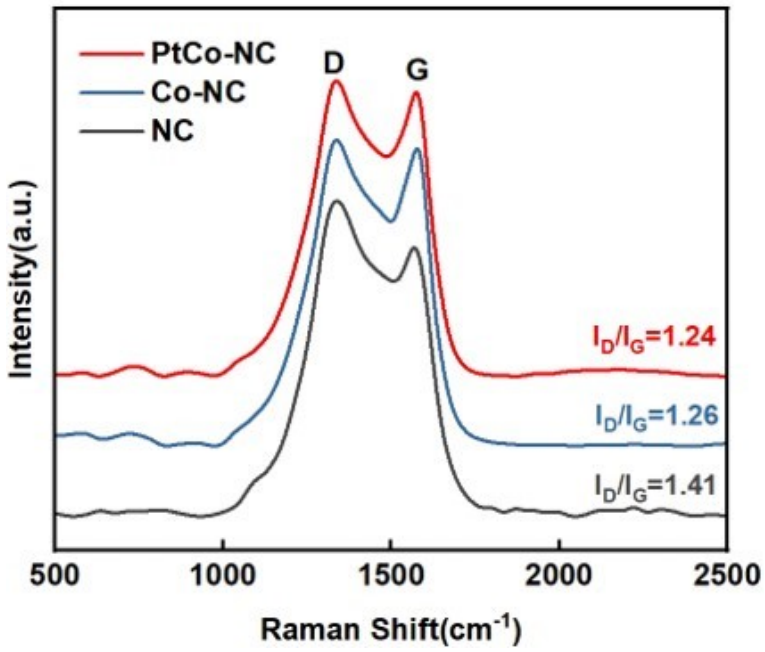


Figure S12. Raman spectra of PtCo-NC, Co-NC and NC

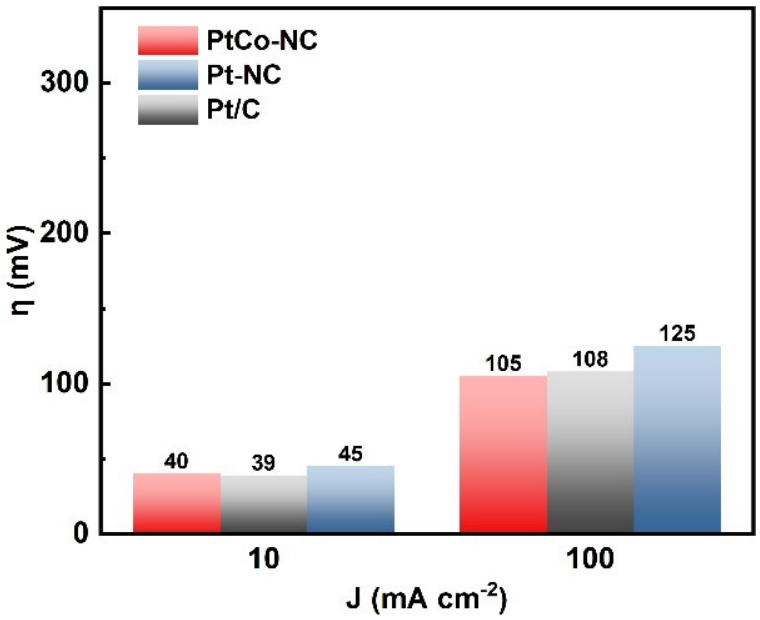


Figure S13. Corresponding overpotentials (j = 10/100 mA $cm^{-2}$) in 0.5 M $H_2SO_4$ of PtCo-NC, Pt-NC and Pt/C

Table S3. The HER performance of the as-prepared catalyst and reported precious metal-based HER electrocatalysts in acidic electrolyte.

| Catalysts | $\eta_{10,100}$ (mV) | Tafel slope (mV $dec^{-1}$) | Mass Activity (@10 mA $cm^{-2}$) | Specific Activity (@10 mA $cm^{-2}$) | TOF ($s^{-1}$@100 mV) | Reference |
|---|---|---|---|---|---|---|
| PtCo-NC | 39, 105 | 28 | 0.15 A $mg_{Pt}^{-1}$ | 1.60 mA $cm^{-2}$ $mg_{Pt}^{-1}$ | 1.40 | This Work |
| Pt/C | 40, 108 | 31 | 0.12 A $mg_{Pt}^{-1}$ | 5.38 mA $cm^{-2}$ $mg_{Pt}^{-1}$ | 1.08 | Commercial |
| PtCo@NC-900 | 46, / | 23 | 4.31 A $mg_{Pt}^{-1}$ | 21.98 mA $cm^{-2}$ $mg_{Pt}^{-1}$ | - | [S1] |
| $Pt_3Co$@NCNT | 42, 70 | 27 | - | - | 1.95 | [S2] |
| Pt/$MoO_2$ | 47, / | 33 | 7.43 A $mg_{Pt}^{-1}$ | - | - | [S3] |
| PtCoFe@CN | 45, / | 32 | - | - | - | [S4] |
| Ru-HPC | 67, / | 67 | 7.80 A $mg_{Ru}^{-1}$ | - | 9.20 | [S5] |
| PtRu/RFCS | 22, 46 | 47 | - | - | 4.00 | [S6] |
| $Pt_3Ni_4$ NWs/C | 40, / | N.A. | - | - | - | [S7] |
| Pt@CIAC-121 | 48, / | 58 | - | - | - | [S8] |

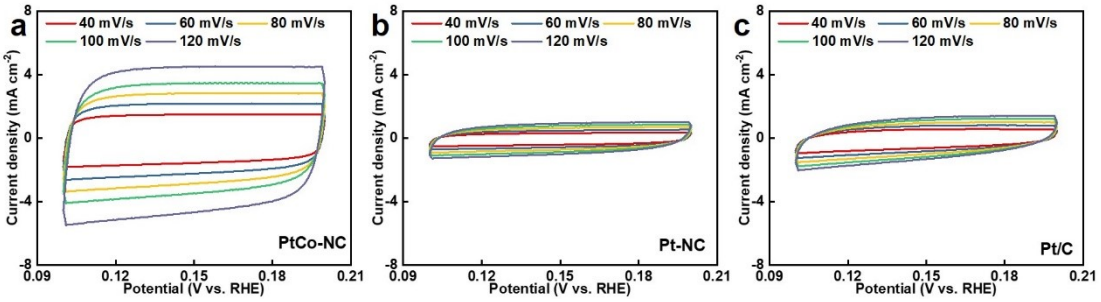


Figure S14. CV curves for PtCo-NC, Pt-NC and Pt/C in 0.5 M $H_2SO_4$ within the potential range of 0.10-0.20 V (V vs. RHE)

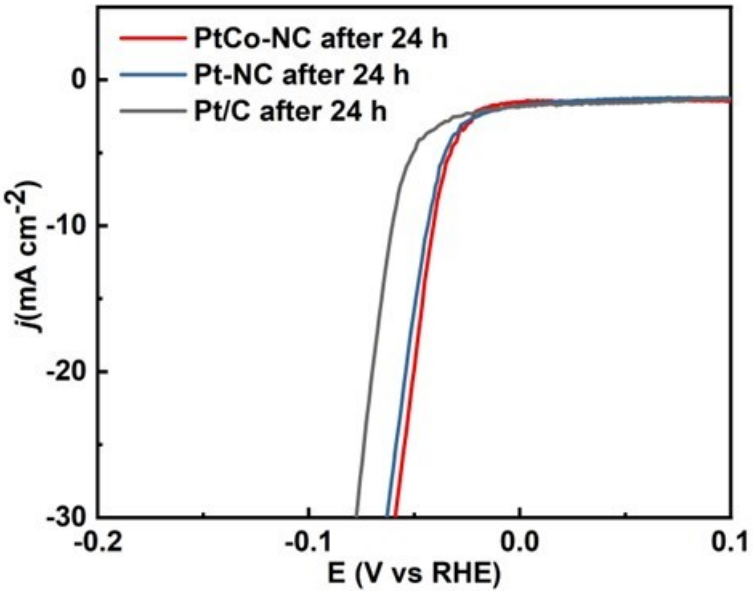


Figure S15. Polarization curves of PtCo-NC, Pt-NC and Pt/C in 0.5 M $H_2SO_4$ after 24 h of operation.

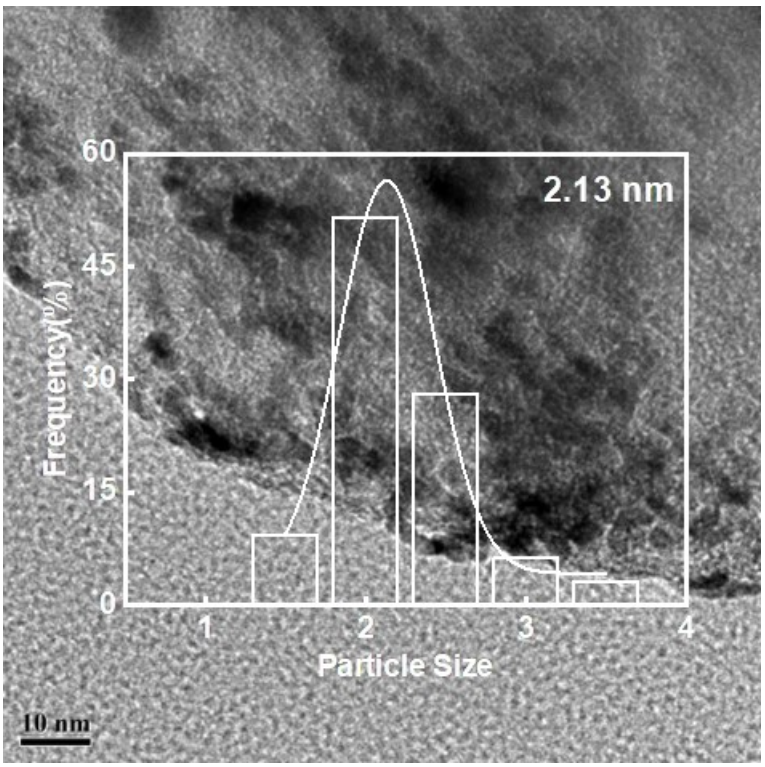


Figure S16. Magnified TEM image of PtCo-NC after stability measurement

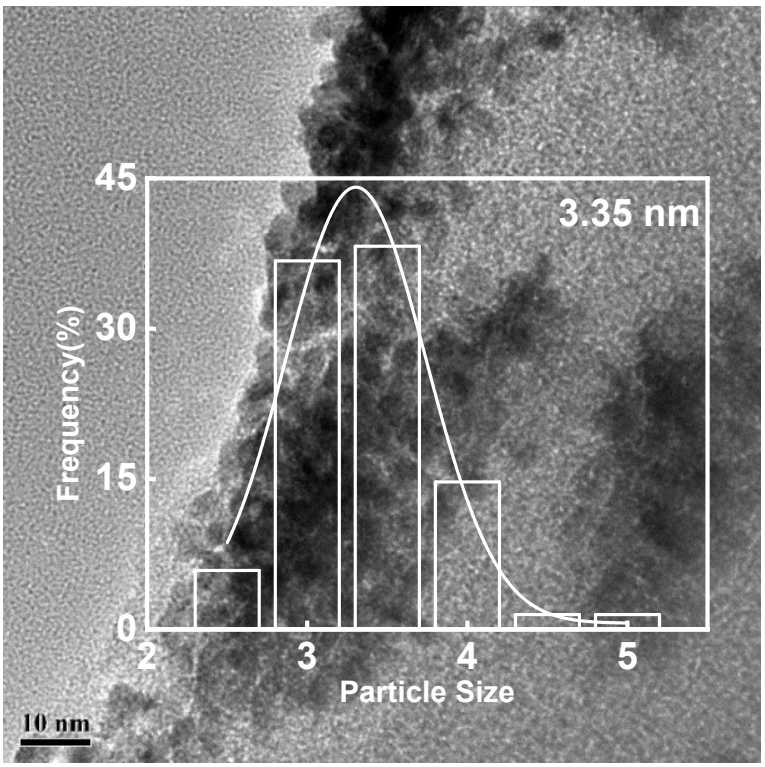


Figure S17. Magnified TEM image of Pt-NC after stability measurement

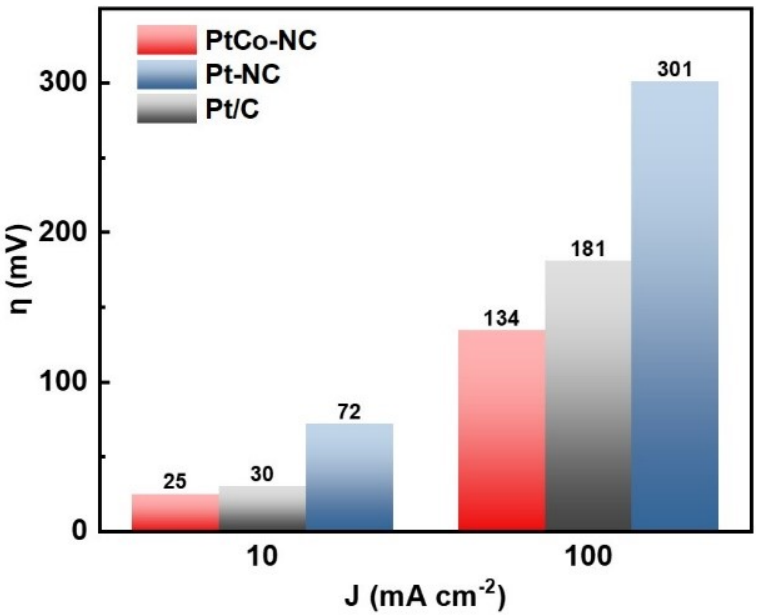


Figure S18. Corresponding overpotentials (j = 10/100 mA $cm^{-2}$) in 1 M KOH of PtCo-NC, Pt-NC and Pt/C

Table S4. The HER performance of the as-prepared catalyst and reported precious metal-based HER electrocatalysts in alkaline electrolyte.

| Catalysts | $\eta_{10,100}$ (mV) | Tafel slope (mV $dec^{-1}$) | Mass Activity (@10 mA $cm^{-2}$) | Specific Activity (@10 mA $cm^{-2}$) | TOF ($s^{-1}$@100 mV) | Reference |
|---|---|---|---|---|---|---|
| PtCo-NC | 25, 134 | 39 | 0.15 A $mg_{Pt}^{-1}$ | 1.49 mA $cm^{-2}$ $mg_{Pt}^{-1}$ | 1.03 | This Work |
| Pt/C | 30, 181 | 45 | 0.12 A $mg_{Pt}^{-1}$ | 2.20 mA $cm^{-2}$ $mg_{Pt}^{-1}$ | 0.70 | Commercial |
| CoPt-$Pt_{SA}$/NDPCF | 31, $199_{300}$ | 44 | 19.30 A $mg_{Pt}^{-1}$ | - | - | [S9] |
| $Pt_3Co$@NCNT | 36, 100 | 35 | - | - | 0.94 | [S2] |
| $Pt_3Fe$/NMCS-A | 29, / | 50 | 0.32 A $mg_{Pt}^{-1}$ | - | 1.32 | [S10] |
| C-ZIF-CuPt | 46, / | 45 | 0.54 A $mg_{Pt}^{-1}$ | - | - | [S11] |
| SA-Ru/Ru NPs/PC | 33, / | 32 | 4.20 A $mg_{Ru}^{-1}$ | - | - | [S12] |
| A-CoPt-NC | 50, / | 48 | 6.43 A $mg_{Pt}^{-1}$ | - | - | [S13] |
| PtNi/C | 42, / | 86 | 7.23 A $mg_{Pt}^{-1}$ | 14.80 mA $cm^{-2}$ $mg_{Pt}^{-1}$ | - | [S14] |

| | | | | | | |
|---|---|---|---|---|---|---|
| PtRu NCs/BP | 64, / | 43 | - | - | - | [S15] |

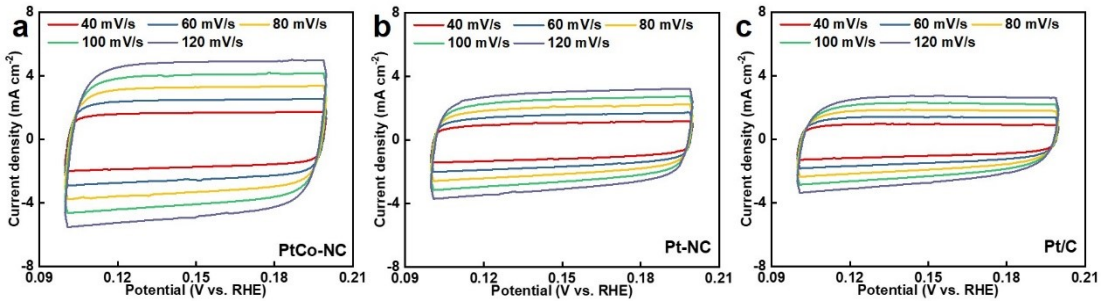


Figure S19. CV curves for PtCo-NC, Pt-NC and Pt/C in 1 M KOH within the potential range of 0.10-0.20 V (V vs. RHE)

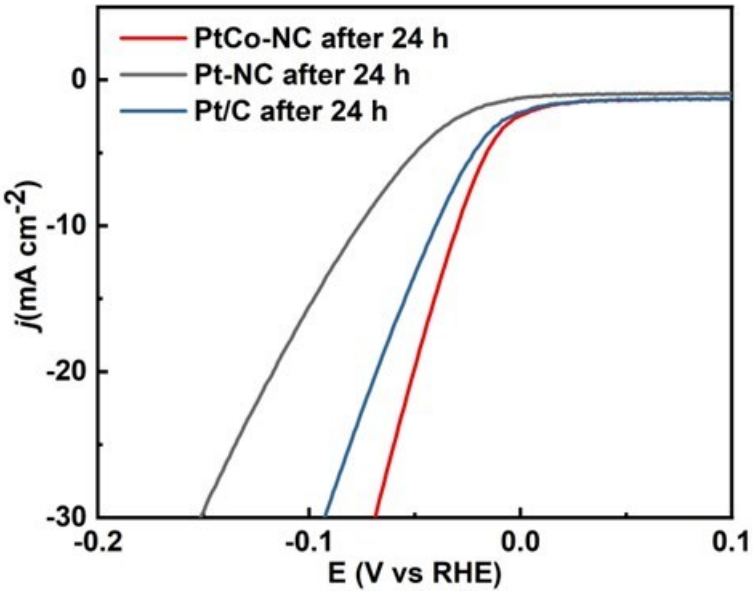


Figure S20. Polarization curves of PtCo-NC, Pt-NC and Pt/C in 1 M KOH after 24 h of operation

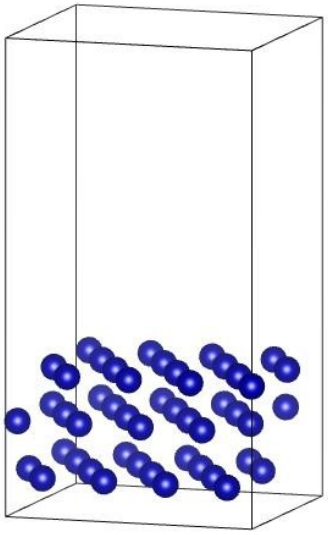

Figure S21. Co (111) slab model

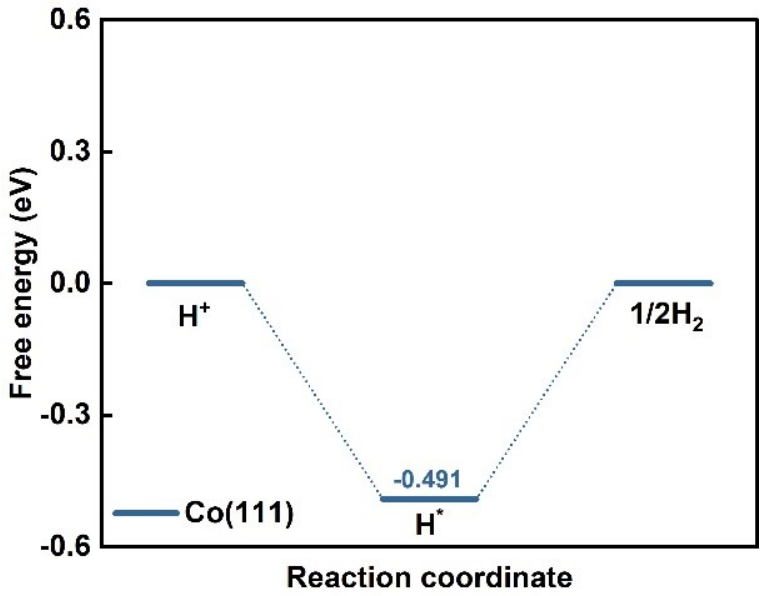

Figure S22. Free-energy of hydrogen adsorption for Co (111)

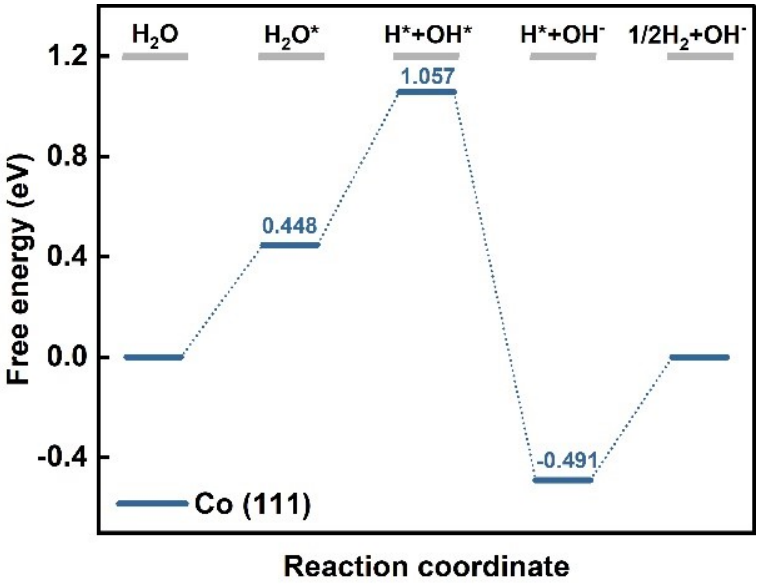


Figure S23. Free-energy of $H_2O$ adsorption for Co (111)

## References

[S1] J. Guo, J. Liu, X. Mao, S. Chu, X. Zhang, Z. Luo, J. Li, B. Wang, C. Jia, D. Qian, Experimental and Theoretical Insights into Enhanced Hydrogen Evolution over PtCo Nanoalloys Anchored on a Nitrogen-Doped Carbon Matrix, The Journal of Physical Chemistry Letters, 13 (2022) 5195-5203.

[S2] S.L. Zhang, X.F. Lu, Z.-P. Wu, D. Luan, X.W. Lou, Engineering Platinum–Cobalt Nano-alloys in Porous Nitrogen-Doped Carbon Nanotubes for Highly Efficient Electrocatalytic Hydrogen Evolution, Angewandte Chemie International Edition, 60 (2021) 19068-19073.

[S3] X. Li, J. Yu, J. Jia, A. Wang, L. Zhao, T. Xiong, H. Liu, W. Zhou, Confined distribution of platinum clusters on MoO2 hexagonal nanosheets with oxygen vacancies as a high-efficiency electrocatalyst for hydrogen evolution reaction, Nano Energy, 62 (2019) 127-135.

[S4] J. Chen, Y. Yang, J. Su, P. Jiang, G. Xia, Q. Chen, Enhanced Activity for Hydrogen Evolution Reaction over CoFe Catalysts by Alloying with Small Amount of Pt, ACS Applied Materials & Interfaces, 9 (2017) 3596-3601.

[S5] T. Qiu, Z. Liang, W. Guo, S. Gao, C. Qu, H. Tabassum, H. Zhang, B. Zhu, R. Zou, Y. Shao-Horn, Highly exposed ruthenium-based electrocatalysts from bimetallic metal-organic frameworks for overall water splitting, Nano Energy, 58 (2019) 1-10.

[S6] K. Li, Y. Li, Y. Wang, J. Ge, C. Liu, W. Xing, Enhanced electrocatalytic performance for the hydrogen evolution reaction through surface enrichment of

platinum nanoclusters alloying with ruthenium in situ embedded in carbon, Energy & Environmental Science, 11 (2018) 1232-1239.

[S7] P. Wang, X. Zhang, J. Zhang, S. Wan, S. Guo, G. Lu, J. Yao, X. Huang, Precise tuning in platinum-nickel/nickel sulfide interface nanowires for synergistic hydrogen evolution catalysis, Nature Communications, 8 (2017) 14580.

[S8] S. Wang, X. Gao, X. Hang, X. Zhu, H. Han, W. Liao, W. Chen, Ultrafine Pt Nanoclusters Confined in a Calixarene-Based $\{Ni_{24}\}$ Coordination Cage for High-Efficient Hydrogen Evolution Reaction, Journal of the American Chemical Society, 138 (2016) 16236-16239.

[S9] W. Yang, P. Cheng, Z. Li, Y. Lin, M. Li, J. Zi, H. Shi, G. Li, Z. Lian, H. Li, Tuning the Cobalt–Platinum Alloy Regulating Single-Atom Platinum for Highly Efficient Hydrogen Evolution Reaction, Advanced Functional Materials, 32 (2022) 2205920.

[S10] P. Kuang, Z. Ni, B. Zhu, Y. Lin, J. Yu, Modulating the d-Band Center Enables Ultrafine $Pt_3Fe$ Alloy Nanoparticles for pH-Universal Hydrogen Evolution Reaction, Advanced Materials, n/a (2023) 2303030.

[S11] C. Wang, L. Kuai, W. Cao, H. Singh, A. Zakharov, Y. Niu, H. Sun, B. Geng, Highly dispersed Cu atoms in MOF-derived N-doped porous carbon inducing Pt loads for superior oxygen reduction and hydrogen evolution, Chemical Engineering Journal, 426 (2021) 130749.

[S12] Q. Hu, G. Li, X. Huang, Z. Wang, H. Yang, Q. Zhang, J. Liu, C. He, Electronic structure engineering of single atomic Ru by Ru nanoparticles to enable enhanced

activity for alkaline water reduction, Journal of Materials Chemistry A, 7 (2019) 19531-19538.

[S13] L. Zhang, Y. Jia, H. Liu, L. Zhuang, X. Yan, C. Lang, X. Wang, D. Yang, K. Huang, S. Feng, X. Yao, Charge Polarization from Atomic Metals on Adjacent Graphitic Layers for Enhancing the Hydrogen Evolution Reaction, Angewandte Chemie International Edition, 58 (2019) 9404-9408.

[S14] Z. Zhao, H. Liu, W. Gao, W. Xue, Z. Liu, J. Huang, X. Pan, Y. Huang, Surface-Engineered PtNi-O Nanostructure with Record-High Performance for Electrocatalytic Hydrogen Evolution Reaction, Journal of the American Chemical Society, 140 (2018) 9046-9050.

[S15] Y. Li, W. Pei, J. He, K. Liu, W. Qi, X. Gao, S. Zhou, H. Xie, K. Yin, Y. Gao, J. He, J. Zhao, J. Hu, T.-S. Chan, Z. Li, G. Zhang, M. Liu, Hybrids of PtRu Nanoclusters and Black Phosphorus Nanosheets for Highly Efficient Alkaline Hydrogen Evolution Reaction, ACS Catalysis, 9 (2019) 10870-10875.